Journal of Sound and Vibration (1999) **224**(2), 305–328
Article No. jsvi.1999.2168, available online at http://www.idealibrary.com on IDEAL®

CLEARANCE EFFECTS ON BILINEAR NORMAL MODE FREQUENCIES

E. A. BUTCHER*

Sandia National Laboratories†, P.O. Box 5800, *MS* 0439, *Albuquerque, NM* 87185-0439, *U.S.A.*

(*Received* 13 *July* 1998, *and in final form* 1 *February* 1999)

The effects of a clearance or interference on the normal mode frequencies of a *n*-dof system with bilinear stiffness and without damping are investigated through various modifications of the bilinear frequency relation. First, the exact penetration distances and bilinear natural frequencies of a single-degree-of-freedom system are analytically obtained in terms of the amount of clearance and the strength of non-linearity, and an equivalent linear system is derived. These results are in turn used to construct three methods which approximate the bilinear frequencies for the *n*-dof system. The specific example of a two-dof system is studied in which the resulting approximate frequencies are compared with those obtained from numerical simulations in order to determine the most accurate approximation technique. The results demonstrate how these bilinear normal mode frequencies vary with the magnitude of the clearance/interference and thus point toward the need of including such effects in methods which utilize the bilinear frequency relation.

1. INTRODUCTION

Clearances exist in many mechanical systems either by design or as the result of wear or failure. In particular, non-linear systems in which the force–displacement curves are approximately piecewise linear usually contain some amount of clearance between the equilibria of the linear subregions and the contact locations which are the borders between these subregions. These systems are of great importance in the modelling of such phenomena as gear backlash, joint dynamics, and cracks in beams and shafts. When the stiffness on one side of the clearance is large, repeated impacts, referred to as vibro-impacts, can lead to large dynamic loads and excessive noise. Accurate knowledge of the system response both to external forces and in free vibration helps in the design and control of the system. The determination of the effect of clearance on the natural

*Present address: Department of Mechanical Engineering, University of Alaska Fairbanks, Fairbanks, AK 99775-5905, U.S.A.

†Sandia National Laboratories is a multiprogram laboratory operated by Sandia Corporation, a Lockheed Martin Company, for the United States Department of Energy under Contract DE-ACO4-94AL85000.

0022–460X/99/270305 + 24 $30.00/0

frequencies and motion of such systems is an important step since resonance occurs when the system is forced at these frequencies.

Since piecewise linear systems are non-linear, they exhibit much of the complicated phenomena associated with non-linear systems. A large amount of literature [1–4] has been written on this subject, most of which deals with one- or two-degree-of-freedom systems with external forcing in the context of modern dynamical systems theory. Rather than pursuing this route, this study concerns the subject of non-linear normal mode frequencies (the non-linear equivalent of linear eigenfrequencies) associated with multi-degree-of-freedom bilinear undamped systems with a non-vanishing clearance.

The treatment of free oscillations of single-degree-of-freedom piecewise linear systems is available in several standard texts [5–7]. In particular, a formula was derived in reference [7] for the period of quarter-symmetric, undamped, free oscillations of a single mass and the effects of clearance variations on the period of the system were briefly outlined. In a recent paper, Todd and Virgin [8] derived the natural frequencies of a single-mass asymmetric bilinear oscillator and included the special case of the impact oscillator with vanishing time of contact. It was shown in their study how both the natural frequency and the penetration distance into the second linear subregion vary with the ratio of the clearance magnitude to the initial amplitude. However, their results were partly incorrect due to the presence of errors (to be discussed) in the mathematical derivation. While the correct solution to the single mass problem has served as the main motivation for the present work, the scope of this paper is extended to include a discussion on techniques for approximating non-linear normal mode (NNM) frequencies of multi-degree-of-freedom bilinear systems with clearances. Of the few papers to deal with clearance effects on multi-degree-of-freedom systems, the focus has primarily dealt directly with the frequency response to external forcing [9].

Since the first investigations of NNMs by Rosenberg [10], it has been a subject of much investigation for various non-linear systems [11]. Until recently, however, few studies on the characteristics of bilinear normal modes (BNMs) existed, mostly due to difficulties associated with the non-smooth aspect of such systems. Three important contributions to the subject include the recent studies of Zuo and Curnier [12], Chen and Shaw [13], and Chati *et al*. [14]. In reference [12] the BNM frequencies were derived using both a numerical technique and an approximate analytical approach for two-degree-of-freedom non-gyroscopic and gyroscopic bilinear systems. The analytical approach utilized the well-known relation for bilinear frequencies of single-degree-of-freedom systems. However, the resulting modal frequencies are independent of the amplitudes and energy in their work because of the lack of a clearance. In reference [13] a method for obtaining the normal modes, associated modal dynamics, and the frequency–amplitude relationship for each mode using invariant manifolds was presented for non-gyroscopic bilinear systems with a non-vanishing clearance. While this technique was applied to a two-degree-of-freedom example, the magnitude of the clearance was fixed so that the effects of clearance variations on the frequencies were not shown. In reference [14] both a perturbation method and another

approximate analytical technique which incorporates the bilinear frequency relation were used in a bilinear two-degree-of-freedom model in order to justify use of the latter method in calculating the natural frequencies of a cracked beam. As in reference [12], however, no clearance between the equilibria and the contact location was present.

The focus of this study is, first, to present the exact solution for the effects of clearance variation on the natural frequency and penetration distance of the single mass problem considered in reference [8] and, second, to present and compare three analytical techniques for approximating the BNM frequencies for multi-degree-of-freedom bilinear systems with clearances. For this purpose, the analytical approximation techniques employed in references [12] and [14] which are based on the bilinear frequency relation are modified to include a non-vanishing clearance while a third similar method is also presented. Unlike in reference [13], the normal modes themselves with their associated dynamics are *not* obtained analytically. The proposed techniques are then applied specifically to a two-mass system in which the resulting BNM frequencies are compared with those obtained from numerical simulations

2. SYSTEM UNDER CONSIDERATION

Consider the n-degree-of-freedom vibrating system shown in Figure 1 whose equations of motion are

$$\begin{gathered} m_1\ddot{x}_1 + f(x_1) - k_1x_2 = 0, \\ m_2\ddot{x}_2 + (k_1 + k_2)x_2 - k_1x_1 - k_2x_3 = 0, \\ \vdots \\ m_n\ddot{x}_n + (k_{n-1} + k_n)x_n - k_{n-1}x_{n-1} = 0, \end{gathered}$$

$$f(x_1) = \begin{Bmatrix} k_1x_1, & x_1 < x_c, \\ (k_1 + k_c)x_1 - k_cx_c, & x_1 > x_c, \end{Bmatrix} \tag{1}$$

where the derivatives are with respect to a time t'. The asymmetric bilinear stiffness of the first mass is plotted in Figure 2 in which it is seen that the overall domain is divided into two distinct linear subregions in which the total energy is always conserved. Unlike the approaches of some researchers, the clearance x_c is *not* restricted to be positive so that a negative clearance, or interference, is also allowed. Both cases are represented in Figure 2. Since the masses' positions are measured from equilibrium, penetration into the second subregion is made only when the energy of the system is sufficient such that the clearance is traversed by the first mass, i.e. $x_1 > x_c$. It will be seen that the bilinear free oscillation

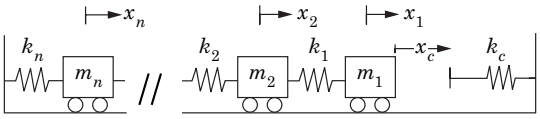

Figure 1. An n-degree-of-freedom bilinear vibrating system with clearance.

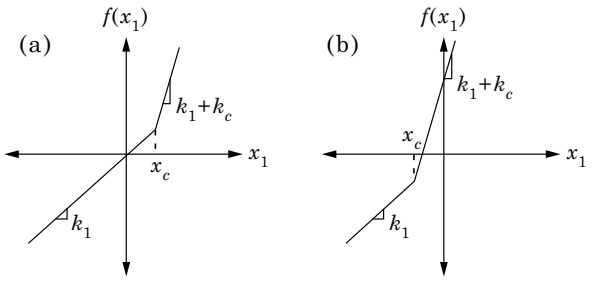

Figure 2. Force versus displacement of the first mass for the cases of (a) clearance and (b) interference.

frequencies depend on both the clearance and the amplitude in this case. Otherwise, if the energy is insufficient for contact with the free spring, then the system remains in the first linear subregion and the solution is easily obtained. In the case of interference, the energy must be sufficient for the first subregion to be obtained (i.e. $x_1 < x_c$); otherwise the system remains continuously in contact with the free spring.

At this point the following scalings are introduced:

$$\mu_i = m_i/m_1, \quad \kappa_i = k_i/k_1, \quad \kappa_c = k_c/k_1, \quad \lambda_{ij} = \kappa_i/\mu_j, \quad \omega_- = \sqrt{k_1/m_1},$$
$$\omega_+ = \sqrt{(k_1 + k_c)/m_1}, \quad t = \omega_- t', \quad \alpha = \omega_+/\omega_- = \sqrt{1 + \kappa_c}, \tag{2}$$

where ω_- and ω_+ are the linear frequencies of vibration of m_1 (with m_2 held still) before and after contact with the free spring, respectively. Equation (1) is now rewritten in matrix form as

$$\begin{bmatrix} \ddot{x}_1 \\ \ddot{x}_2 \\ \vdots \\ \ddot{x}_n \end{bmatrix} + \begin{bmatrix} K_{11} & -1 & 0 & 0 \\ -\lambda_{12} & \lambda_{12} + \lambda_{22} & -\lambda_{22} & 0 \\ & & & \\ 0 & \vdots & \vdots & \vdots \\ 0 & 0 & -\lambda_{(n-1)n} & \lambda_{(n-1)n} + \lambda_{nn} \end{bmatrix} \begin{bmatrix} x_1 \\ x_2 \\ \vdots \\ x_n \end{bmatrix} = \begin{bmatrix} F_1 \\ 0 \\ 0 \\ 0 \end{bmatrix},$$

$$K_{11} = \begin{Bmatrix} 1, & x_1 < x_c, \\ \alpha^2, & x_1 > x_c, \end{Bmatrix}, \quad F_1 = \begin{Bmatrix} 0, & x_1 < x_c, \\ \kappa_c x_c, & x_1 > x_c, \end{Bmatrix} \tag{3}$$

or

$$\ddot{\mathbf{x}} + \mathbf{K}\boldsymbol{x} = \mathbf{F}, \tag{4}$$

where the derivatives are now with respect to the dimensionless time t. Equation (4) may be solved to obtain solutions $\mathbf{x}_-(t)$ and $\mathbf{x}_+(t)$ before and after contact, respectively, and the entire solution for the bilinear system is obtained by matching these solutions at $x = x_c$.

3. SINGLE-DEGREE-OF-FREEDOM BILINEAR SYSTEM

The single-degree-of-freedom version of equation (4) is

$$\ddot{x} + K_{11}x = F_1, \tag{5}$$

where K_{11} and F_1 are defined in equation (3). This is the same problem which was considered by Todd and Virgin [8] and their procedure is also used here. In what follows, the mass is assumed to be released from rest at a given distance to the left of the equilibrium position in the $x < x_c$ subregion. Therefore, for given initial conditions $x(0) = -x_0$ and $\dot{x}(0) = 0$, the solution in this region is

$$\begin{bmatrix} x_-(t) \\ \dot{x}_-(t) \end{bmatrix} = \begin{bmatrix} -x_0 \cos t \\ x_0 \sin t \end{bmatrix}, \tag{6}$$

which yields the circle

$$x_-^2 + \dot{x}_-^2 = x_0^2 \tag{7}$$

in the phase plane. (Note that an ellipse is generated in real time.) Of course, if contact is made with the free spring, then only the portion for which $x < x_c$ is present while the connecting portion for $x > x_c$ is an ellipse whose precise shape is determined from the solution in the second subregion. When multiplied through by 1/2, equation (7) is also a statement of conservation of the total energy $E = x_0^2/2$.

Because of the presence of the non-homogeneous term in equation (5), the solution after contact is made must include a particular solution and can in general be written as

$$\begin{bmatrix} x_+(t) \\ \dot{x}_+(t) \end{bmatrix} = \begin{bmatrix} A\sin(\alpha t) + B\cos(\alpha t) + x_e \\ A\alpha\cos(\alpha t) - B\alpha\sin(\alpha t) \end{bmatrix}, \tag{8}$$

where A and B are to be found and

$$x_e = [\kappa_c/(1+\kappa_c)]x_c = (1 - 1/\alpha^2)x_c \tag{9}$$

is the mathematical equilibrium position in the second subregion. In the elastic rebound limit ($\alpha \to \infty$) it is equal to the clearance. Notice that x_e is a physical equilibrium of the bilinear system only if the clearance is negative, i.e., $x_c < 0$, while the origin is the true physical equilibrium if $x_c > 0$. In the latter case x_e would be the physical equilibrium if the mass was "glued" to the free spring.

It should be pointed out that one of the errors in the analysis presented in reference [8] was the omission of a particular solution in the second subregion, a situation which results in a non-physical stiffness discontinuity at $x = x_c$. As seen in Figure 2, the actual stiffness is everywhere continuous. The impact condition is $x_-(t_c) = x_c$ such that the time of impact is found as

$$t_c = \cos^{-1}(-\rho), \tag{10}$$

where $\rho = x_c/x_0$ is the ratio of the clearance to the initial displacement magnitude and must lie in the interval $[-1, 1]$ if contact/separation is to occur.

Since x_0 is assumed positive, an interference results in a negative value of this ratio and contact occurs before the system reaches the origin. If $\rho > 1$ then the clearance is too large for contact to occur and the system remains in the first linear subregion while if $\rho < -1$ then the system remains in the second linear subregion. For $-1 < \rho < 1$ the distance D_- traversed by the mass before contact occurs can be expressed in dimensionless form in terms of ρ as

$$D_-/x_0 = 1 + \rho. \tag{11}$$

The displacement and velocity matching conditions (i.e. $x_+(t_c) = x_c$ and $\dot{x}_+(t_c) = \dot{x}_-(t_c)$) at the point of contact require that

$$\begin{bmatrix} \sin(\alpha t_c) & \cos(\alpha t_c) \\ \alpha\cos(\alpha t_c) & -\alpha\sin(\alpha t_c) \end{bmatrix} \begin{bmatrix} A \\ B \end{bmatrix} = \begin{bmatrix} x_c - x_e \\ x_0 \sin(t_c) \end{bmatrix}. \tag{12}$$

The solution of this system results in an oscillation amplitude in the second subregion given by

$$C = \sqrt{A^2 + B^2} = (x_0/\alpha)\sqrt{1 - \rho^2(1 - 1/\alpha^2)}, \tag{13}$$

whilst the maximum displacement is $C + x_e$ from equation (8). This gives the ellipse

$$\alpha^2(x_+ - x_e)^2 + \dot{x}_+^2 = \alpha^2 C^2 = x_0^2 - x_c x_e \tag{14}$$

with center at $(x_+, \dot{x}_+) = (x_e, 0)$ in the phase plane which is matched to the circle of equation (7) at $x_- = x_+ = x_c$, as shown in Figure 3 for both the clearance and interference cases. Here, the dashed line represents the switching plane between the linear subregions and the dot identifies the point $(x_e, 0)$. Since the total energy $E = x_0^2/2$ remains constant, the potential energy in the second subregion can be found from equation (14) as $V = (\alpha^2(x_+ - x_e)^2 + x_c x_e)/2$.

To find the actual penetration distance D_+ into the second subregion, x_c is subtracted from the maximum displacement to obtain

$$D_+ = C + x_e - x_c = (x_0/\alpha)\sqrt{1 - \rho^2(1 - 1/\alpha^2)} - x_c/\alpha^2. \tag{15}$$

Dividing by the initial displacement magnitude x_0, equation (15) is expressed in terms of the dimensionless parameters α and ρ as

$$D_+/x_0 = (1/\alpha)\sqrt{1 - \rho^2(1 - 1/\alpha^2)} - \rho/\alpha^2 \tag{16}$$

for $-1 < \rho < 1$ while the penetration distance is zero if $\rho > 1$. This is graphed versus the clearance as the solid lines in Figure 4 for a variety of different values of α. The dashed line represents the distance traversed before contact given by equation (11). The total distance traversed by the mass during a half-period is the sum of these, i.e.,

$$(D_- + D_+)/x_0 = 1 + (1/\alpha)\sqrt{1 - \rho^2(1 - 1/\alpha^2)} + \rho(1 - 1/\alpha^2). \tag{17}$$

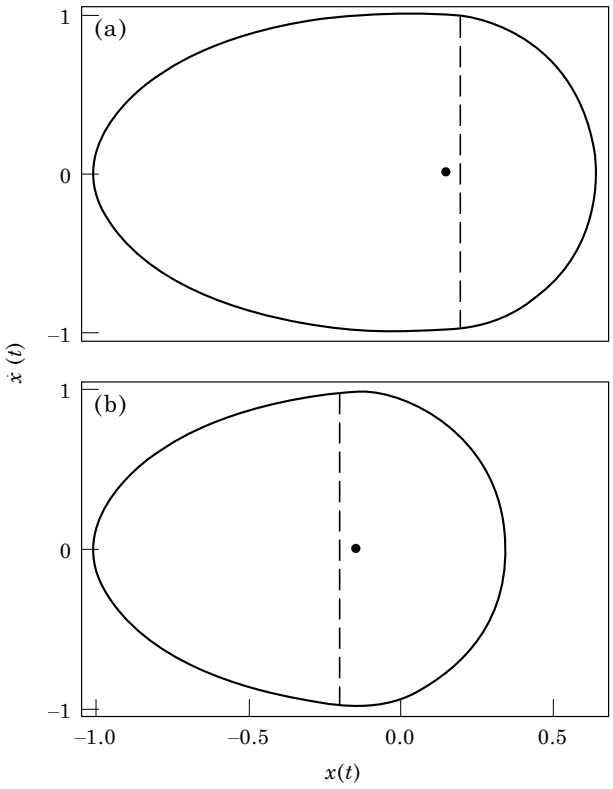

Figure 3. Phase plane portraits for the single-degree-of-freedom bilinear system for the cases of (a) clearance ($\alpha = 2$, $\rho = 0{\cdot}2$) and (b) interference ($\alpha = 2$, $\rho = -0{\cdot}2$). The dashed line represents the switching plane and the point is the equilibrium position of the second subregion.

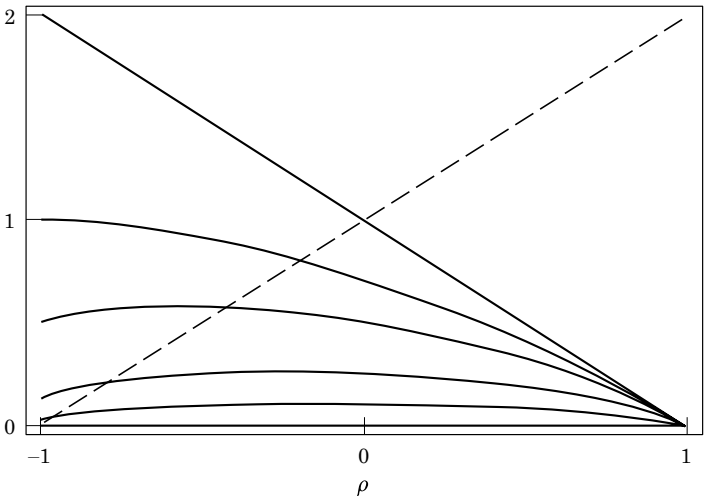

Figure 4. Traversal distance for the single-degree-of-freedom bilinear system as a function of clearance in the first subregion (D_-/x_0, ---) and the second subregion (penetration distance D_+/x_0, —) for (top to bottom) $\alpha = 1$, $\sqrt{2}$, 2, 4, 10 and ∞.

It should be pointed out that the results in equations (13–16) do not agree with those obtained in reference [8] because of the previously mentioned omission of the particular solution in that study. In addition, the authors' use of the absolute value of x_c (neglecting its sign) in equation (15) results in the penetration distance being non-physically symmetric with respect to ρ.

For a given value of α, the value of ρ which results in the largest penetration distance into the second subregion is found by setting $\partial(D_+/x_0)/\partial\rho$ to zero. For $\kappa_c > 1$ ($\alpha^2 > 2$) this results in

$$\rho_{max} = -\sqrt{1/(\alpha^2 - 1)}, \tag{18}$$

whereas $\rho_{max} = -1$ when $1 < \alpha^2 < 2$ as seen in Figure 4. Thus, the largest penetration occurs for an interference with magnitude less than x_0 only when the stiffness of the free spring is greater than that of the attached one (i.e., $k_c > k_1$); otherwise, it occurs when $x_c = -x_0$ and the system always remains in the second linear subregion. These results are in contrast to those presented in reference [8] in which the maximum penetration was said to occur when $\rho = 0$ (i.e., vanishing clearance) regardless of the value of α. However, it is seen from equation (18) that $\rho_{max} = 0$ only in the limit as $\alpha \to \infty$ (i.e., as the contact spring becomes rigid). Since this is the elastic rebound case of vanishing time of contact (vibro-impact), there is no penetration when $\alpha = \infty$ regardless of ρ as demonstrated in Figure 4. Substitution of ρ_{max} into equation (16) yields the maximum penetration into the second subregion as

$$\left(\frac{D_+}{x_0}\right)_{max} = \left\{ \begin{array}{cc} \sqrt{1/(\alpha^2 - 1)}, & \alpha^2 > 2, \\ 2/\alpha^2, & 1 < \alpha^2 < 2. \end{array} \right\} \tag{19}$$

Equations (18) and (19) are plotted in Figure 5 as the solid and dashed lines, respectively.

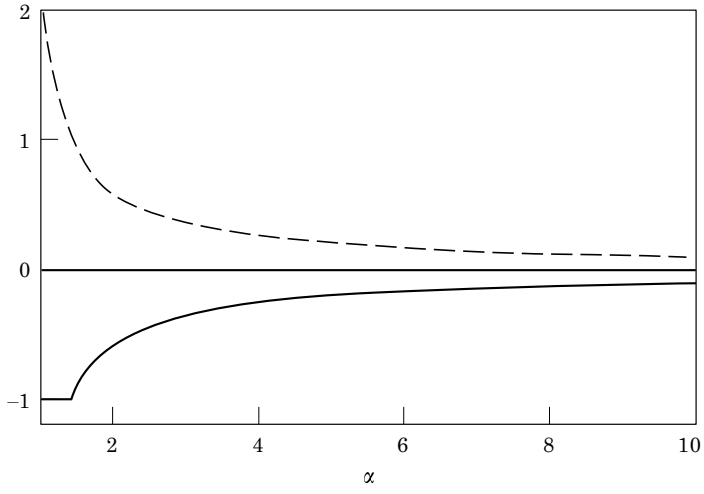

Figure 5. The value of $\rho_{\max}$ (—) which results in the maximum penetration distance ($(D_+/x_0)_{\max}$, - - -) as a function of the bilinear frequency ratio for the single-degree-of-freedom system.

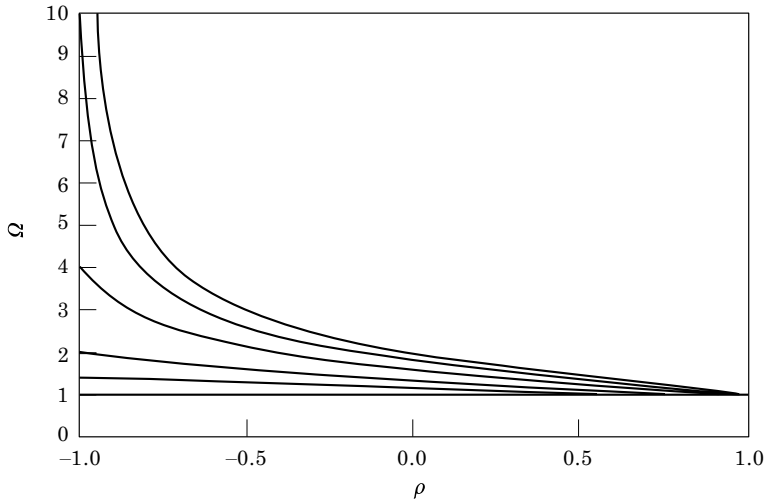

Figure 6. Bilinear natural frequencies for the single-degree-of-freedom system as a function of clearance for (bottom to top) $\alpha = 1$, $\sqrt{2}$, 2, 4, 10 and ∞.

The total period of the mass is the sum of the partial periods of each of the two subregions and can be found by integrating over the closed path Γ as

$$T = \oint_{\Gamma} \mathrm{d}t = T_- + T_+ = 2\int_{-x_0}^{x_c} \frac{1}{\dot{x}_-}\,\mathrm{d}x_- + 2\int_{x_c}^{C+x_e} \frac{1}{\dot{x}_+}\,\mathrm{d}x_+ \tag{20}$$

in terms of the orbits in the phase plane given by equations (7) and (14) from which the velocities in the above integrals are determined. Evaluation of these integrals using equations (9) and (13) yields the period as

$$T = 2[\pi/2 + \sin^{-1}\rho + (1/\alpha)(\pi/2 - \sin^{-1}(\rho/(\alpha\sqrt{1-\rho^2(1-1/\alpha^2)})))], \tag{21}$$

from which the bilinear natural frequency is obtained as

$$\Omega = 2\pi/T. \tag{22}$$

Ω is plotted versus ρ in Figure 6 for various values of α. Again, equations (21, 22) are different from the frequency derived in reference [8] for the same reasons as mentioned above.

When $\alpha = 1$, no change of stiffness is felt between subregions and the frequency is independent of the clearance or amplitude. If the clearance vanishes ($\rho = 0$), then equation (22) simplifies to

$$\Omega = 2/(1 + 1/\alpha), \tag{23}$$

which runs from 1 to 2 as α increases from 1 to ∞, the latter case being the elastic rebound limit where the natural frequency has doubled from that of totally free oscillation. Also, $\Omega = 1$ when $\rho = 1$ and $\Omega = \alpha$ when $\rho = -1$ since the system continuously remains in the respective subregions. As $\alpha \to \infty$, equation (22) becomes

$$\Omega = 2/(1 + (2/\pi)\sin^{-1}\rho), \tag{24}$$

which is represented by the topmost curve in Figure 6. This curve represents the asymptotic limit for any given clearance as a higher frequency is not possible. It should be pointed out that these frequencies are in normalized time. In real time ω_- is also multiplied in equations (22) and (23) which become

$$\Omega = 2\omega_-\omega_+\left[\omega_+\left(1+\frac{2}{\pi}\sin^{-1}\rho\right)+\omega_-\left(1-\frac{2}{\pi}\sin^{-1}\left(\frac{\rho}{\alpha\sqrt{1-\rho^2(1-1/\alpha^2)}}\right)\right)\right]^{-1} \tag{25}$$

and

$$\Omega = 2\omega_-\omega_+/(\omega_+ + \omega_-) \tag{26}$$

respectively. Equation (26) is the well-known "bilinear frequency relation" and has appeared in many studies of bilinear systems which do not contain a clearance (e.g. references [1, 12, 14]).

An equivalent linear system may now be constructed. For this purpose, the original bilinear spring system is replaced with one linear spring which has a stiffness $k_{eq} = \Omega^2$ in normalized time or $k_{eq} = m_1\Omega^2$ in real time. When equation (26) for vanishing clearance is used, this results in

$$k_{eq} = m_1\Omega^2 = 4(1/\sqrt{k_-} + 1/\sqrt{k_+})^{-2} \tag{27}$$

in terms of the stiffness before ($k_- = k_1$) and after ($k_+ = k_1 + k_c$) impact. In normalized time, the equivalent linear stiffness including clearance effects is

$$k_{eq} = \Omega^2 = 4\left(\left\{1+\frac{2}{\pi}\sin^{-1}\rho\right\}+\frac{1}{\alpha}\left\{1-\frac{2}{\pi}\sin^{-1}\left(\frac{\rho}{\alpha\sqrt{1-\rho^2(1-1/\alpha^2)}}\right)\right\}\right)^{-2}, \tag{28}$$

where it should be recognized by analogy to equation (27) that the normalized stiffnesses before and after impact for vanishing clearance are $k_- = 1$ and $k_+ = \alpha^2$, respectively. The terms enclosed in braces { } may be interpreted as the "correction factors" to these stiffnesses to account for the effects of the non-vanishing clearance. Hence, the "corrected" stiffnesses before and after impact are

$$\tilde{k}_- = \{1 + (2/\pi)\sin^{-1}\rho\}^{-2} \tag{29}$$

and

$$\tilde{k}_+ = \alpha^2\left\{1-\frac{2}{\pi}\sin^{-1}\left(\frac{\rho}{\alpha\sqrt{1-\rho^2(1-1/\alpha^2)}}\right)\right\}^{-2} \tag{30}$$

respectively.

Finally, having obtained the period of motion, the complete solution for $t > 0$ can be expressed as

$$x(t) = \left\{ \begin{array}{ll} x_-(t - iT), & iT - t_c < t < iT + t_c, \\ x_+(t - iT), & iT + t_c < t < (i+1)T - t_c, \end{array} \right\}, \quad i = 0, 1, 2, \ldots, \tag{31}$$

where $x_-(t)$ and $x_+(t)$ are given in equations (6) and (8), respectively. The penetration distances and natural frequencies given here were compared with those obtained via numerical simulation of equation (5) and to those given in reference [8]. The present results agreed with those from the simulations with an accuracy determined by the numerical time step while those of reference [8], as expected, did not agree for non-vanishing clearances. For the simulation, a "fitting" procedure was utilized wherein the equations of motion were integrated using a fourth-order Runge–Kutta (R–K) algorithm with a constant time step until contact with the free spring was detected. At this point one Euler integration step was performed using the exact time step needed to reach the boundary after which the R–K procedure was continued but with a smaller time step to account for the increased stiffness. This procedure was also used for release from the free spring after which use of the original time step was resumed. Results confirmed that the energy remains constant across the contact boundary.

4. APPROXIMATE METHODS FOR THE MULTI-DEGREE-OF-FREEDOM BILINEAR SYSTEM

4.1. BILINEAR NORMAL MODE CHARACTERISTICS

The multi-degree-of-freedom bilinear system in Figure 1 is now considered. One desires to find the BNM frequencies of the system as a function of the clearance and stiffness of the free spring. For this purpose, three different approximation techniques which are derived from the bilinear frequency relation are considered. Each contains adjustments to account for a clearance or interference. First, however, some of the characteristics of BNMs are reviewed for the reader.

1. While the motions associated with most initial conditions of bilinear systems are quasiperiodic or even chaotic, the motions of BNMs are *periodic* in time. Hence, resonance occurs when the system is forced at the associated frequencies or, since the motions are in general not sinusoidal, integral multiples of these frequencies.

2. The trajectories of BNMs in the configuration space are *open curves* (instead of straight lines in the linear case) which, in contrast to NNMs of smooth non-linear systems, *neither pass through the origin nor are orthogonal at their intersection*. Although the displacements do not vanish simultaneously, they do reach their maxima and minima at the same time, however.

3. If the clearance is zero, then the BNM frequencies are constant and independent of the energy level since the nonlinearity is concentrated at the

origin. For a *non-zero* clearance, however, *the frequencies depend on the energy* (initial amplitude).

4. For *weak* non-linearities, i.e., small $(\alpha - 1)$, *the number of structurally stable BNMs is generally equal to the number of linear modes for non-resonant cases*. Unlike the case for smooth non-linear systems, sufficient conditions for the existence and uniqueness of normal modes for bilinear systems are not available (although a necessary condition is given in reference [13]). As the strength of non-linearity increases, therefore, additional BNMs which have increasingly more complicated motions may occur along with regions of chaotic behavior.

4.2. PIECEWISE MODAL METHOD

In reference [14], Chati *et al.* utilized the bilinear frequency relation in approximating the natural frequencies of both a two-degree-of-freedom bilinear system and a cracked beam. In each example, the eigenfrequencies in each subregion were found via a linear eigenanalysis (a finite element package was utilized for the beam) and used in the bilinear frequency relation of equation (26). The resulting natural frequencies obtained using this procedure are

$$\Omega_i = 2\omega_{-i}\omega_{+i}/(\omega_{+i} + \omega_{-i}), \tag{32}$$

where ω_{-i} and ω_{+i} are the eigenfrequencies before and after contact, respectively. The associated period is the sum of the half-periods of these individual linear modes, while the associated motion consists of the splicing together of the half-eigenvectors of the linear modes. This is an approximation rather than an exact result since, if initial conditions were chosen corresponding to the ith linear normal mode in the first subregion, then once contact occurs the motion would consist of a superposition of all associated linear modes in the second subregion rather than just the ith mode [14]. For the two-degree-of-freedom system the approximate bilinear frequencies were shown to be reasonable when the strength of non-linearity was small, however, since the initial conditions for the BNM would be close to that of the ith linear normal mode in the first subregion. As the non-linearity (free spring stiffness) was increased, the approximated bilinear frequencies diverged from those obtained using numerical simulation, as did those obtained using a perturbation approach.

This procedure can be modified to include a clearance by first finding the equilibrium vector $\mathbf{x}_e$ in the second subregion as a function of the total number n of masses. Using a static analysis in Figure 1 this can be found for the kth mass as

$$x_{ke} = [(n - k + 1)(\alpha^2 - 1)/(n(\alpha^2 - 1) + 1)]x_c, \tag{33}$$

which reduces to equations (9) when $n = 1$. The motion of the first mass in the ith linear normal mode in each subregion can be written as

$$\begin{bmatrix} x_{1-}(t) \\ \dot{x}_{1-}(t) \end{bmatrix} = \begin{bmatrix} -x_{10}\cos(\omega_{-i}t) \\ x_{10}\omega_{-i}\sin(\omega_{-i}t) \end{bmatrix} \tag{34}$$

and

$$\begin{bmatrix} x_{1+}(t) \\ \dot{x}_{1+}(t) \end{bmatrix} = \begin{bmatrix} A\sin(\omega_{+i}t) + B\cos(\omega_{+i}t) + x_{1e} \\ A\omega_{+i}\cos(\omega_{+i}t) - B\omega_{+i}\sin(\omega_{+i}t) \end{bmatrix}, \tag{35}$$

where A and B are to be found. The displacement and velocity matching conditions of the first mass at the moment of contact then result in

$$\begin{bmatrix} \sin(\gamma_i\beta) & \cos(\gamma_i\beta) \\ \gamma_i\cos(\gamma_i\beta) & -\gamma_i\sin(\gamma_i\beta) \end{bmatrix} \begin{bmatrix} A \\ B \end{bmatrix} = \begin{bmatrix} x_c - x_{1e} \\ x_{10}\sin(\beta) \end{bmatrix}, \tag{36}$$

where $\beta = \cos^{-1}\rho$, $\rho = x_c/x_{10}$ and $\gamma_i = \omega_{+i}/\omega_{-i}$ is the ratio of the eigenfrequencies in the ith mode before and after contact. The solution of this system results in an oscillation amplitude for the first mass in the second subregion given by

$$C = \sqrt{A^2 + B^2} = (x_{10}/\gamma_i)\sqrt{1 - \rho^2(1 - (\gamma_i/[n(\alpha^2 - 1) + 1])^2)}, \tag{37}$$

while the penetration distance of mass 1 into the second subregion is given by

$$\frac{D_+}{x_{10}} = \frac{1}{\gamma_i}\sqrt{1 - \rho^2\left(1 - \left(\frac{\gamma_i}{n(\alpha^2 - 1) + 1}\right)^2\right)} - \frac{\rho}{n(\alpha^2 - 1) + 1}. \tag{38}$$

The above equations reduce to equations (13) and (16) when $n = 1$ since $\alpha = \gamma_i$ in that case. The normalized frequency is found by integrating over the closed path as in equation (20) to yield

$$\Omega_i = \pi\omega_{-i}\left[\frac{\pi}{2} + \sin^{-1}\rho + \frac{1}{\gamma_i}\left(\frac{\pi}{2} - \sin^{-1}\left(\frac{\gamma_i\rho}{(n(\alpha^2 - 1) + 1)\sqrt{1 - \rho^2(1 - (\gamma_i/[n(\alpha^2 - 1) + 1])^2)}}\right)\right)\right]^{-1}, \tag{39}$$

which reduces to equation (22) for $n = 1$. Equation (39) can thus be used to obtain approximate BNM frequencies for bilinear systems with clearance as equation (32) was used for systems without a clearance in reference [14]. However, because the eigenvectors in each subregion match only if the clearance vanishes, for a non-vanishing clearance the displacements and velocities of masses 2–n are discontinuous at the instant that mass 1 (whose displacement and velocity remain continuous) impacts the free spring. It will be seen that the magnitude of the discontinuity (and therefore the accuracy of the approximated frequency) varies with the mode.

Although two sets of eigenfrequencies must initially be computed in general, for the special cases in which formulas for the modal frequencies in each linear subregion exist, equation (39) may be used to obtain similar formulas for the approximate modal frequencies of the bilinear system. As an example, for a uniform n-DOF mass–spring lattice the λ_{ij}'s in equation (3) are unity and the

eigenfrequencies before contact are known from the dispersion relation to be $\omega_{-i} = 2\ \sin[(2i-1)\pi/(4n+2)]$ which are enclosed in the interval [0, 2]. In addition, if $\alpha = \sqrt{2}$ such that the free spring has the same stiffness as the others, then the eigenfrequencies after contact are similarly known as $\omega_{+i} = 2\ \sin[i\pi/(2n+2)]$ such that $\gamma_i = \sin[i\pi/(2n+2)]/\sin[(2i-1)\pi/(4n+2)] > 1$ and the approximate bilinear modal frequencies are directly obtained from equation (39). For a vanishing clearance this reduces to

$$\Omega_i = 2\omega_{-i}/(1+1/\gamma_i) = 2\omega_{+i}/(1+\gamma_i), \tag{40}$$

where ω_{-i}, ω_{+i} and γ_i are given above. Since $\gamma_i > 1$, equation (40) states that each Ω_i is contained in the interval $[\omega_{-i}, \omega_{+i}]$. As $i \to n$, $\gamma_i \to 1$ and this interval shrinks with Ω_i approaching both ω_{-i} and ω_{+i}. The same approach can be used with other spatially periodic lattices. For a non-vanishing clearance, it is expected that the BNM frequencies satisfy the "compatibility conditions" that $\Omega_i \in [\omega_{-i}, \omega_{+i}]$ for $\rho \in [-1, 1]$ and $\Omega_i \to \omega_{-i}$ and ω_{+i} as $\rho \to 1$ and -1, respectively. However, equation (39) does not satisfy these conditions. This apparent discrepancy can be better understood by examining the resulting frequencies for the uniform lattice above when n/i becomes large. Then $\gamma_i \to 2i/(2i-1)$, $x_{1e} \to x_c$, and the lower bilinear modal frequencies are approximated by

$$\Omega_i = \frac{2\omega_{-i}\omega_{+i}}{\omega_{+i}(1+(2/\pi)\sin^{-1}\rho)+\omega_{-i}} = \left(\frac{i(i-\frac{1}{2})}{(1+(1/\pi)\sin^{-1}\rho)i-\frac{1}{4}}\right)\frac{\pi c}{L}, \tag{41}$$

where $\omega_{-i} = (i-1/2)\pi c/L$ and $\omega_{+i} = i\pi c/L$ are the natural frequencies for longitudinal vibrations of fixed–free and fixed–fixed bars, respectively, in terms of the wavespeed (c) and length (L). When $\rho = 0$ it can be easily shown that $\Omega_i \in [\omega_{-i}, \omega_{+i}]$ and becomes more linear as i increases. However, it can also be seen that equation (41) does not satisfy the compatibility conditions above for a non-vanishing clearance. In fact, for a fixed $\rho \neq 0$ this approximation quickly breaks down as the mode number i increases. A better approximation would be $\Omega_i = i(i-1/2)/[i-(1-(2/\pi)\sin^{-1}\rho)/4]\ (\pi c/L)$ which in fact does satisfy the above compatibility conditions. Apparently equation (39) requires similar modification. In any case, it can be seen that, unlike its linear counterparts, the BNM frequencies depend on the total energy through the presence of ρ (which depends on the initial amplitude).

4.3. GLOBAL EQUIVALENT LINEAR STIFFNESS METHOD

Zuo and Curnier [12] presented an approximate analytical approach for obtaining the BNM frequencies for a bilinear multi-degree-of-freedom system with vanishing clearance by constructing a linear system whose natural frequencies approximate that of the bilinear system. For this purpose, they directly extended the concept of obtaining an equivalent linear stiffness by postulating an equivalent stiffness matrix

$$\mathbf{K}_{eq} = 4(\mathbf{K}_-^{-1/2} + \mathbf{K}_+^{-1/2})^{-2} \tag{42}$$

by analogy with equation (27), where $\mathbf{K}_-$ and $\mathbf{K}_+$ are the stiffness matrices

before and after contact which have leading (top-left-most) elements k_- and k_+, respectively. The solution of the eigenvalue problem $|\mathbf{K}_{eq} - \omega_{eq}^2 \mathbf{M}| = 0$ is then utilized to obtain the approximate BNM frequencies ω_{eq}. In their study, these were found to be accurate only when the strength of non-linearity $\delta = \omega_+ - \omega_- = (\alpha - 1)\omega_-$ was small, and the resulting frequencies for two-degree-of-freedom non-gyroscopic and gyroscopic systems were plotted up to $\delta = 2$. For high values of δ, their approximate BNM frequencies diverged from those obtained via a numerical iteration technique.

This formulation may also be extended to include clearances by using the "corrected" stiffnesses $\tilde{k}_-$ and $\tilde{k}_+$ given by equations (29) and (30) as the leading elements in the associated stiffness matrices. This results in the equivalent stiffness matrix

$$\mathbf{K}_{eq} = 4(\tilde{\mathbf{K}}_-^{-1/2} + \tilde{\mathbf{K}}_+^{-1/2})^{-2} \tag{43}$$

in normalized time in which the stiffness matrices themselves are "corrected" to account for non-vanishing clearances. The approximate BNM frequencies are then given by the solution of the eigenvalue problem $|\mathbf{K}_{eq} - \omega_{eq}^2 \mathbf{I}| = 0$ since the masses were incorporated in the stiffness matrix in equation (3). In contrast with the piecewise modal method for approximating the BNM frequencies, only one set of eigenfrequencies must be calculated using this technique. Since the matrix elements in $\mathbf{K}_{eq}$ in general differ from the corresponding ones in $\mathbf{K}_-$ and $\mathbf{K}_+$, the presence of a clearance affects the equivalent stiffness matrix *globally*. As a result, the effects of the clearance are not easily seen in this matrix. In addition, several problems arise with this method which preclude its effective use under certain conditions. These include the fact that above or below certain values of ρ, the pre- and post-impact "corrected" stiffness matrices are not positive definite so that their square roots in equation (43) are not defined. (This result is not physical, of course; it results from the manner in which the clearance effects are introduced.) Also, the results show non-physical clearance variations in the frequencies of both modes for $\alpha = 1$, the linear case where the results are expected to be most accurate. In general, the results diverge as the magnitude of ρ increases and the compatibility conditions described above are not observed. Hence, this method is only effective for small non-linearities *and* clearances. Because it requires taking matrix roots and inverses, it is also necessary from a practical standpoint that the dimension of the system be small.

4.4. LOCAL EQUIVALENT LINEAR STIFFNESS METHOD

In order to extend the accuracy of the previous method to larger clearances, another approach for assembling the equivalent linear stiffness matrix is sought. To this end it is recognized that, in contrast with equations (42) and (43), only the leading element of $\mathbf{K}_{eq}$ should be affected by the presence of the free spring. Since the problem of determining this matrix element was solved in section 3, the equivalent stiffness matrix in normalized time for this approximation is the $\mathbf{K}$ matrix in equation (3) with k_{eq} from equation (28) replacing K_{11} as the leading element. This is not only more straightforward than equation (43) but also

results in more accurate BNM frequencies for bilinear systems with a large non-vanishing clearance/interference. By thus altering an individual stiffness matrix element *locally* as needed from the solution to a one-dof problem, the effect of the clearance on each mass of the system is easily seen in $\mathbf{K}_{eq}$ while the effects on the frequencies properly diminish as the dimension of the multi-dof system is increased. The solution of the eigenvalue problem $|\mathbf{K}_{eq} - \omega_{eq}^2 \mathbf{I}| = 0$ then yields the approximate BNM frequencies ω_{eq} for both modes. In general, the approximate frequencies will overestimate the true ones and thus serve as an upper bound as in the Ritz method. For the limiting linear cases of $\rho = \pm 1$, however, the results are exact. Furthermore, $\Omega_i \in [\omega_{-i}, \omega_{+i}]$ for $\rho \in [-1, 1]$ so that the compatibility conditions are satisfied. As with the previous method, only one set of eigenfrequencies must be calculated. For any value of α, however, the frequencies obtained using this approximation are more accurate for large clearances than those obtained using equation (43). In addition, the method can be easily implemented for high dimensional systems.

5. EXAMPLE: TWO-DEGREE-OF-FREEDOM BILINEAR SYSTEM

The three methods of section 4 are now applied to the two-degree-of-freedom bilinear system obtained by considering only the motion of the first two masses of Figure 1 with mass 3 held rigid. The values of λ_{12} and λ_{22} in equation (3) are set to unity. The total energy of the system is found from the initial potential energy

$$E = \tfrac{1}{2}[x_{10} \quad x_{20}] \begin{bmatrix} 1 & -1 \\ -1 & 2 \end{bmatrix} \begin{bmatrix} x_{10} \\ x_{20} \end{bmatrix} = \tfrac{1}{2}(x_{10}^2 + 2x_{20}^2 - 2x_{10}x_{20}), \tag{44}$$

while the potential energy in the second subregion is $V = (x_{2+}^2 + (x_{1+} - x_{2+})^2 + (\alpha^2 - 1)(x_{1+} - x_c)^2)/2$. In order to assess the accuracy of the three approximation techniques, their results are compared with those obtained via numerical simulation of the two-mass system using the same algorithm as described in section 3. Figure 7 shows the simulation results in the configuration space for a variety of different clearances and interferences with total energy $E = 1$ and $\alpha^2 = 2$. In each case, the smaller closed solid curve represents the maximum equipotential boundary inside which the motion must remain while the large ellipse represents the corresponding boundary in the absence of the free spring. The open dashed curves are the BNMs. The first and last cases are completely linear and the corresponding normal modes are straight lines as expected. It is seen in several cases that three period 1 BNMs are present. (Period k BNMs cross the boundary between subregions k times in a half-period.) Two of them, the short-dashed and long-dashed modes, will be called BNM 1a and BNM 1b since the motions of each approach those of the first linear normal mode at $\rho = 1$ and -1 (the first and last cases), respectively. It is seen that, unlike a similar 2-DOF example in reference [13], the normal modes in this problem do not uniquely correspond to the linear ones. As BNM 1a and 1b approach $\rho = -1$ and 1, respectively, a bifurcation into higher period BNMs (represented by the additional solid curves in Figures 7(d) and 7(h)) occurs

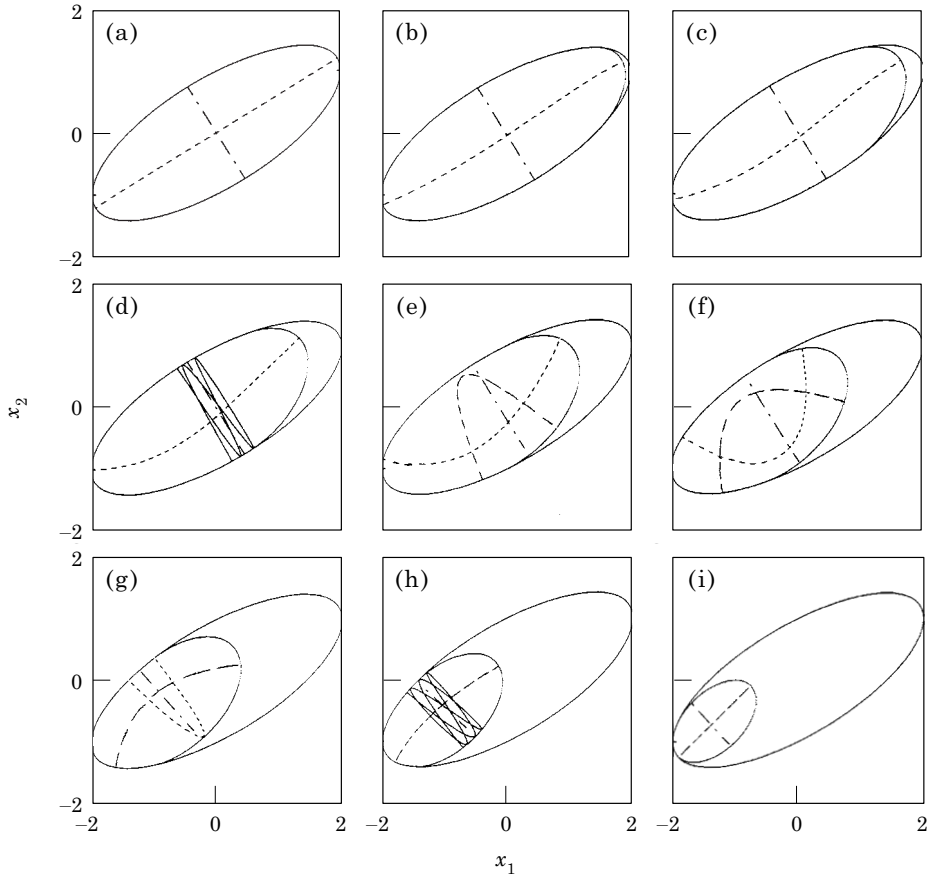

Figure 7. Numerical simulations in configuration space of BNM 1a (----), BNM 1b (– – –), and BNM 2 (— · —) with $\alpha = \sqrt{2}$ and x_c = (a) 2·0, (b) 1·5, (c) 1·0, (d) 0·5, (e) 0·0, (f) −0·5, (g) −1·0, (h) −1·5, (i) −2·0 for the two-degree-of-freedom bilinear system. The solid closed curves are the maximum equipotential boundaries with and without the free spring while the additional solid curves in (d) and (h) represent bifurcations to higher period BNMs.

before they are absorbed into the second linear normal mode. The short-long-dashed mode is BNM2 since it approaches the second linear normal mode at both $\rho = 1$ and -1. This occurs for a *smaller* clearance/interference than in BNM 1a,b since the amplitudes of mass 1 are smaller.

The initial conditions for the BNM simulations were found by trial and error. For each different x_c case, the parameter ρ was computed separately for each mode and the frequencies were obtained from the simulation. The results are tabulated in Table 1. An important issue is how the parameter ρ is defined. While $\rho = x_c/x_{10}$ is sufficient for BNMs 1a and 2, a more general definition is required for BNM 1b since the fact that the initial motion of this mode is in the negative x_1 direction may lead to ambiguous values of ρ greater than 1 even though the boundary between subregions is still crossed. By defining $\rho = x_c/x_{1*}$ where x_{1*} is the *maximum penetration if the free spring were removed*, the resulting values of ρ are consistent for this mode. It should be noted that the two

TABLE 1
BNM frequencies from numerical simulations

	BNM 1a		BNM 1b		BNM 2	
x_c	ρ	Ω	ρ	Ω	ρ	Ω
−2·0	–	–	−1·047	1·0	–	–
−1·5	–	–	−0·750	0·962	−1·031	1·732
−1·0	−0·714	0·854	−0·571	0·906	−0·833	1·714
−0·5	−0·275	0·805	−0·323	0·862	−0·541	1·679
−0·375	–	–	–	–	−0·436	1·673
−0·25	−0·129	0·781	−0·161	0·845	−0·316	1·663
−0·125	–	–	–	–	−0·174	1·652
0·0	0·0	0·758	0·0	0·830	0·0	1·645
0·125	–	–	0·150	0·823	0·211	1·637
0·25	0·125	0·737	0·374	0·816	0·472	1·627
0·375	–	–	–	–	0·781	1·620
0·5	0·25	0·717	–	–	1·110	1·618
1·0	0·503	0·679	–	–	–	–
1·5	0·761	0·643	–	–	–	–
2·0	1·027	0·618	–	–	–	–

definitions of ρ are equivalent for BNMs 1a and 2 since the initial motion in these modes is in the positive x_1 direction. Also, the present convention of calculating the frequency as a function of the ratio of the clearance to the peak displacement of mass 1 is very similar to the form of the results in reference [13] in which the clearance was fixed. The numerical BNM frequencies of Table 1 are plotted as a function of ρ in Figure 8 as the dots connected by short-dashed lines. It is seen that BNMs 1a and 1b exist simultaneously for most of the region. Since each of the three approximation methods can yield only two BNM frequencies, it is expected that an accurate approximation for the first modal frequency will closely track those of BNMs 1a and 1b for high and low values of ρ, respectively, while migrating from one to the other somewhere in between. As can be seen, this accurately describes the results of the piecewise modal and local equivalent linear stiffness methods.

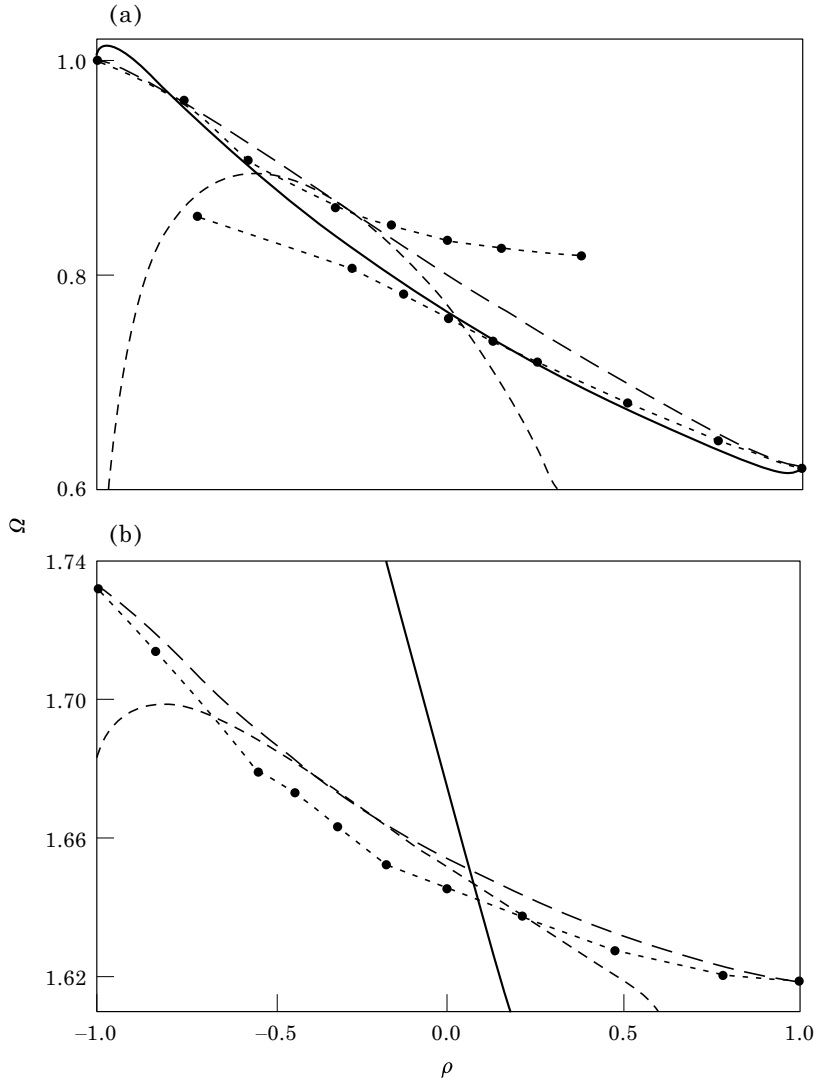

Figure 8. Bilinear natural frequencies for the two-degree-of-freedom system in (a) BNM 1a-b and (b) BNM 2 computed via the piecewise modal method (———), global (– – – –) and local (— — —) equivalent linear stiffness methods, and numerical simulations (●- - - -●) as a function of clearance for $\alpha = \sqrt{2}$. The BNM 1a (for $-0{\cdot}714 \leqslant \rho \leqslant 1{\cdot}0$) simulation frequencies are lower than those of BNM 1b (for $-1{\cdot}0 \leqslant \rho \leqslant 0{\cdot}374$) for a given ρ.

The piecewise modal method yields the approximate BNM frequencies by equation (39). The linear normal mode frequencies before contact are $\omega_{-1,2} = 0{\cdot}618,\ 1{\cdot}618$, while those after contact are found in terms of α as

$$\omega_{+1,2} = \sqrt{[\alpha^2 + 2 \mp \sqrt{\alpha^4 - 4\alpha^2 + 8}]/2}. \tag{45}$$

For $\alpha^2 = 2$ they are $\omega_{+1,2} = 1{\cdot}0,\ 1{\cdot}732$ while $\gamma_{1,2} = 1{\cdot}618,\ 1{\cdot}070$. These linear frequencies are evident in Figure 8 at $\rho = 1$ and -1. Since the motion is assumed to lie on the eigenvectors in each subregion, equation (44) may be used to

express ρ as a function of the total energy in each of the two BNMs as $\rho = x_c/(1{\cdot}9465\sqrt{E})$ for the first mode and $\rho = x_c/(0{\cdot}4595\sqrt{E})$ for the second mode. The resulting frequencies are plotted as the solid lines in Figure 8 in which it is seen that this technique is much more accurate for the first mode than for the second. As was discussed in section 4.2, this is because of the greater discontinuity in the displacement and velocity of mass 2 which occur at the boundary between subregions in the second mode. This can be seen by attempting to match the linear eigenvectors at the point of contact. While this can be accomplished for the first mode with little discontinuity for any value of ρ, the resulting gap between the eigenvectors of the second mode quickly becomes large as the magnitude of ρ increases. Consequently, the method yields reasonable frequencies for the second mode only within a very small band near $\rho = 0$ (or actually closer to $\rho = 0{\cdot}1$).

The global equivalent linear stiffness method yields the equivalent stiffness matrix as

$$\mathbf{K}_{eq} = 4\left(\begin{bmatrix} \tilde{k}_- & -1 \\ -1 & 2 \end{bmatrix}^{-1/2} + \begin{bmatrix} \tilde{k}_+ & -1 \\ -1 & 2 \end{bmatrix}^{-1/2}\right)^{-2}, \tag{46}$$

where the "corrected" stiffnesses are given in equations (29) and (30) with $\alpha^2 = 2$ and the BNM frequencies are determined from $|\mathbf{K}_{eq} - \omega_{eq}^2\mathbf{I}| = 0$. For 200 equally-spaced values of ρ, the resulting frequencies were computed and are plotted as medium-dashed lines in Figure 8 in which it is seen that this technique is more accurate for larger regions of interferences than clearances in both modes. On both sides of these regions the approximations rapidly drop off. In fact, equation (46) does not give any real frequencies for $\rho > 0{\cdot}6$ in either mode since the submatrices above do not remain positive definite past this point. It is also seen that the method is accurate for a larger range of ρ in the second mode than in the first.

The local equivalent linear stiffness method yields a different equivalent stiffness matrix as

$$\mathbf{K}_{eq} = \begin{bmatrix} k_{eq} & -1 \\ -1 & 2 \end{bmatrix}, \tag{47}$$

where k_{eq} is given in equation (28) with $\alpha^2 = 2$ and the BNM frequencies are also determined from $|\mathbf{K}_{eq} - \omega_{eq}^2\mathbf{I}| = 0$. Again, for 200 values of ρ the resulting frequencies were computed and are plotted as long-dashed lines in Figure 8. It is apparent here that, although the other methods may be more accurate at certain points in one mode or the other, the results from this technique lie closer to the numerically computed frequencies over the whole range of ρ in both modes than do those of the other methods. In addition, the compatibility conditions discussed in section 4.2 are satisfied. Hence, this technique was utilized to plot the BNM frequencies of both modes as functions of ρ for several values of α in Figure 9. A good qualitative understanding of the effects of clearance variations on BNM frequencies may be obtained from this figure, which is similar to that (Figure 6) for the single mass problem. It is seen that, while the frequencies in

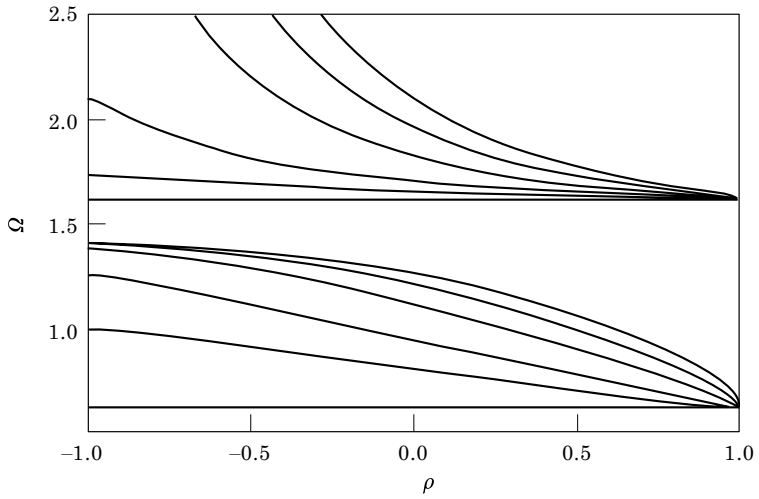

Figure 9. Bilinear natural frequencies for the two-degree-of-freedom system computed via the local equivalent linear stiffness method as a function of clearance for (bottom to top in both modes) $\alpha = 1$, $\sqrt{2}$, 2, 4, 10 and ∞.

both modes increase with a decrease in ρ, those for the first mode approach an asymptotic limit of $\sqrt{2} = 1{\cdot}41$ for $\rho = -1$ as $\alpha \to \infty$ while those for the second mode approach α. As in Figure 6, the results of Figure 9 are independent of ρ when $\alpha = 1$ and all of the first and second mode frequencies uniformly approach the values of 0·618 and 1·618, respectively, when $\rho = 1$. In contrast, the results obtained from the global equivalent linear stiffness method do not conform to these expected results.

The small errors in the results from the local equivalent linear stiffness method result from the approximated frequencies overestimating the true ones as in the Ritz method. As anticipated, these deviations occur mainly around $\rho = 0$ while the BNM frequencies are exact at $\rho = \pm 1$. These errors increase with an increase in α as shown in Figure 10 in which the BNM frequencies computed via the three methods are plotted as a function of α for zero clearance along with those obtained from numerical simulations. These simulations are qualitatively similar to those in Figure 7 but are not shown here (except for those corresponding to $\alpha = \sqrt{2}$ which appear in Figure 7(e)). It should be noticed that, if little clearance is present, then one of the other methods gives more accurate results, while the local equivalent linear stiffness method is obviously more reliable in predicting the BNM frequencies for systems with large clearances. As α becomes very large and vibro-impact results, however, the dynamics can be much more complicated with BNMs of higher period occurring in between regions of chaotic behavior [14]. In that case it is questionable how much useful information can be obtained from any of the present approximation techniques which are better suited to systems with smaller nonlinearities.

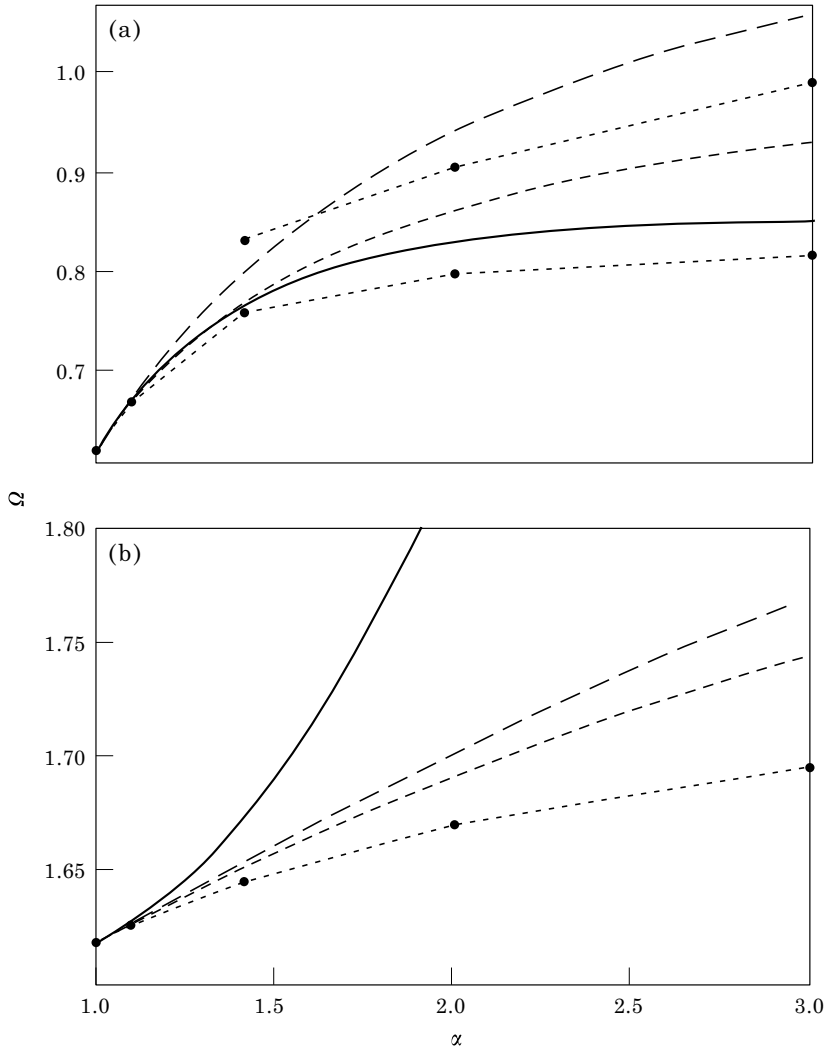

Figure 10. Bilinear natural frequencies for the two-degree-of-freedom system in (a) BNM 1a-b and (b) BNM2 computed via the piecewise modal method (——), global (– – –) and local (— — —) equivalent linear stiffness methods, and numerical simulations (●- - -●) as a function of α for zero clearance. The BNM 1a (for $\alpha \geqslant 1{\cdot}0$) simulation frequencies are lower than those of BNM 1b (for $\alpha \geqslant 1{\cdot}41$) for a given ρ.

6. CONCLUSIONS

The effects of a clearance on the normal mode frequencies of a system with bilinear stiffness were investigated. First, the exact penetration distances and bilinear natural frequencies of a single-degree-of-freedom system were analytically obtained in terms of the amount of clearance and the strength of non-linearity, and an equivalent linear system (with the same frequency) was derived. The formula for the natural frequencies was shown to reduce to the well-known bilinear frequency relation for vanishing clearance. The results were exact (to computational accuracy) when compared to those obtained from

numerical simulations. Three approximate methods for obtaining the bilinear frequencies for the n-dof system including clearance effects were then outlined and the resulting frequencies were compared with those obtained from numerical simulations of a two mass system. The latter revealed three distinct modes for $\alpha = \sqrt{2}$, two of which are perturbations of the first linear mode for different ranges of clearance/interference. In the piecewise modal method, the bilinear frequency relation employing the linear modal frequencies in each of the linear subregions as in reference [14] was directly modified to include a non-zero clearance/interference. The resulting frequencies were very good in the first bilinear mode but poor in the second due to large discontinuities at the instant of contact. In the two equivalent linear stiffness methods (the first of which was based on a technique for zero clearance utilized in reference [12]), an equivalent linear stiffness matrix was constructed and the resulting eigenfrequencies were determined. The ''global'' version was more accurate for systems with little clearance while the ''local'' version was more accurate for systems with a large clearance or interference since the results were exact at the two ends in which the problem becomes completely linear.

The local equivalent linear stiffness method was also used to construct Figure 9 which demonstrates how the clearance magnitude affects the bilinear frequencies of both modes for a variety of different stiffnesses of the free spring. Errors resulting from an overestimation of the true frequencies appeared mostly for large non-linearities and small clearance magnitudes. This diagram, which is similar in many ways to that (Figure 6) obtained for the single mass system, provides a good qualitative picture of the clearance effects in each of the bilinear normal modes and points toward the need for including such effects in methods which utilize the bilinear frequency relation. For example, the piecewise modal method was based on the technique employed in reference [14] which utilized the bilinear frequency relation in calculating the natural frequencies of a cracked beam. In that study, two finite element models of the beam (with the crack open and closed) were constructed from which the two separate sets of modal frequencies were obtained for use in equation (32). Since a clearance was not included, the results were appropriate for a thin crack which is closed at static equilibrium and open only during bending, or in other words when the boundary between linear subregions passes through the origin in the configuration space. However, for a wider crack which is also open at equilibrium the presence of the clearance between the crack faces requires the inclusion of its effects in the approximation since the resulting bilinear modal frequencies will be *smaller* than those resulting from a thin crack. Although any of the three methods discussed here could theoretically be utilized to include the clearance effects in the finite element model, it is observed that relatively little effort would be required to use the piecewise modal method in conjunction with standard finite element packages as was done in reference [14]. The local equivalent linear stiffness method, on the other hand, would require code specifically tailored to the problem since certain individual elements of the stiffness matrices (those corresponding to the degrees of freedom associated with the nodes on the crack faces) would require separate modifications. The greater

accuracy of the results obtained from this technique for the two mass system (especially for the higher mode) may justify the development of such code, however. The previously-mentioned limitations of the global equivalent linear stiffness method makes that technique incompatible with a large finite element problem.

ACKNOWLEDGMENTS

The author is appreciative of the comments and suggestions of Drs. Daniel Segalman and Clark Dohrmann which contributed toward the paper.

REFERENCES

1. S. W. Shaw and P. J. Holmes 1983 *Journal of Sound and Vibration* **90**, 129–155. A periodically forced piecewise linear oscillator.
2. H. S. Choi and J. Y. K. Lou 1991 *International Journal of Non-Linear Mechanics* **26**, 461–473. Non-linear behavior and chaotic motions of an sdof system with piecewise-non-linear stiffness.
3. S. L. Lau and W.-S. Zhang 1992 *Journal of Applied Mechanics* **59**, 153–160. Nonlinear vibrations of piecewise-linear systems by incremental harmonic balance method.
4. M. Kleczka, E. Kreuzer and W. Schiehlen 1992 *Philosophical Transactions of the Royal Society of London* **A 339**, 533–546. Local and global stability of a piecewise linear oscillator.
5. N. Minorksi 1947 *Non-linear Mechanics*. Michigan: Edward Brothers.
6. A. A. Andronov, A. A. Vitt and S. E. Khaikin 1966 *Theory of Oscillators*. Oxford: Pergamon Press.
7. S. Timoshenko 1955 *Vibration Problems in Engineering*. New York: D. Van Nostrand.
8. M. D. Todd and L. N. Virgin 1996 *Journal of Sound and Vibration* **194**, 452–460. Natural frequency considerations of an impact oscillator.
9. R. J. Comparin and R. Singh 1990 *Journal of Sound and Vibration* **142**, 101–124. Frequency response characteristics of a multi-degree-of-freedom system with clearances.
10. R. M. Rosenberg 1962 *Journal of Applied Mechanics* **30**, 7–14. The normal modes of nonlinear *n*-degrees-of-freedom-systems.
11. A. F. Vakakis, L. I. Manevitch, Y. V. Mikhlin, V. N. Pilipchuk and A. A. Zevin 1996 *Normal Modes and Localization in Nonlinear Systems*. New York: John Wiley.
12. L. Zuo and A. Curnier 1994 *Journal of Sound and Vibration* **174**, 289–313. Nonlinear real and complex modes of conewise linear systems.
13. S.-L. Chen and S. W. Shaw 1996 *Nonlinear Dynamics* **10**, 135–164. Normal modes for piecewise linear vibratory systems.
14. M. Chati, R. Rand and S. Mukherjee 1997 *Journal of Sound and Vibration* **207**, 249–270. Modal analysis of a cracked beam.